QCD AT FINITE TEMPERATURE AND DENSITY

M. D'Elia[a] and M.P. Lombardo[b]

[a] **Dept. of Physics and INFN - Genova - Italy**

[b] **INFN - Padova - Italy**

SMFT 2002 – Bari, September 26 - 28, 2002

OUTLINE

- Lattice QCD at finite density
- The imaginary chemical potential method
- Results obtained in four flavour QCD
- Conclusions and Perspectives

1 – Introduction

At zero chemical potential the QCD partition function can be easily discretized on an euclidean lattice with finite temporal extent $\tau = 1/T$

$$Z = \int \mathcal{D}U \mathcal{D}\psi \mathcal{D}\bar{\psi} e^{-(\beta S_G + S_F)} = \int \mathcal{D}U e^{-\beta S_G} \det M[U] \quad (1)$$

$U, \psi, \bar{\psi} \longrightarrow$ gauge link and fermionic variables

$S_G \longrightarrow$ pure gauge action

$S_F = \bar{\psi} M[U] \psi \longrightarrow$ fermionic action

$M[U] \longrightarrow$ fermionic matrix

At non-zero chemical potential μ, the temporal gauge links appearing in the integrand in Eq. (1) are modified as follows (a is the lattice spacing):

$$U_t \rightarrow e^{a\mu} U_t \qquad\qquad U_{-t} \rightarrow e^{-a\mu} U_{-t} \quad (2)$$

This transformation does not change S_G, but $\det M[U]$ gets a complex phase $\Longrightarrow$ importance sampling and standard lattice MonteCarlo simulations are unfeasible

If the chemical potential is purely imaginary, $\mu = i\mu_I$

$$U_t \rightarrow e^{ia\mu_I} U_t \qquad\qquad U_{-t} \rightarrow e^{-ia\mu_I} U_{-t} = (e^{ia\mu_I} U_t)^\dagger \quad (3)$$

$\det M[U]$ is again real and positive, simulations are feasible. However one is giving up the original aim of simulating finite density QCD, so:

Why are simulations at imaginary chemical potential interesting, apart from the fact that they are feasible?

Is it possible to obtain information relevant for finite density QCD from simulations at imaginary chemical potential ?

1.1 – Analytic continuation to real μ

$Z(T, \mu)$ is analytic and even in μ when away from phase transitions.

$$\log Z(\mu) = a_0 + a_2\mu^2 + a_4\mu^4 + O(\mu^6) \tag{4}$$

$$\log Z(i\mu_I) = a_0 - a_2\mu_I^2 + a_4\mu_I^4 + O(\mu_I^6) \tag{5}$$

Simulations at small μ_I can be used to determine the expansion coefficients for the free energy and other physical quantities.

The method is expected to work well in the region of interest for present experiments (RHIC, LHC), i.e. that of high temperatures and small chemical potential ($T \sim T_c \sim 160$ MeV, $\mu/T \sim 0.1$).

It has been already studied:
in the strong coupling regime (M.P. Lombardo, 2000)
in dimensionally reduced 3–d QCD theory (Hart, Laine, Philipsen, 2001)
and in two flavours QCD (Ph. de Forcrand and O. Philipsen, 2002)

Results obtained in this way can then be cross-checked with those obtained by reweighting techniques (Z. Fodor and S.D. Katz, 2002) and by direct measurements of the derivatives with respect to μ at $\mu = 0$ (C.R. Allton *et al*, 2002; S. Choe *et al*, 2002)

1.2 – Reconstruction of the canonical partition function

$Z(T, i\mu_I)$ can also be used to reconstruct the canonical partition function $Z(V, T, n)$ at fixed quark number n (A. Roberge and N. Weiss, 1986)
Using the identity:

$$Z(T,n) = \frac{1}{2\pi} \int_0^{2\pi} \mathrm{d}\theta e^{-i\theta n} Z(T, i\theta T) \ . \tag{6}$$

where $\theta = \mu_I/T$. As n grows, the factor $e^{-i\theta n}$ oscillates more and more rapidly and the error in the numerical integration grows exponentially.

The method has been tested in the 2–d Hubbard model up to $n = 6$ (M. G. Alford, A. Kapustin, F. Wilczek, 1999).

No attempt has still be done for QCD.

1.3 – T–μ_I phase diagram

The study of the phase diagram in the T–μ_I plane provides guidance to the analytic continuation to real chemical potential and it is moreover an interesting physical problem by itself.

The phase structure in the $(T, i\mu_I)$ plane has been first predicted by Roberge and Weiss using strong and weak coupling calculations.

Let us consider the grand canonical partition function

$$Z(T, i\mu_I) = \mathrm{Tr}\left(e^{\frac{i\mu_I \hat{N}}{T}} e^{-\frac{\hat{H}_{\mathrm{QCD}}}{T}}\right)$$

$\hat{H}_{\mathrm{QCD}} \longrightarrow$ QCD Hamiltonian
$\hat{N} = \int d^3x \psi^\dagger \psi \longrightarrow$ quark number operator

$\hat{N}$ is a number operator, so Z is surely periodic in μ_I/T with period 2π. A period $2\pi/N_c$ is expected only in the confined phase, with N_c the number of colors, since there only physical states with $\langle \hat{N} \rangle$ multiple of N_c are present.

However, Roberge and Weiss have shown that $Z(T, i\mu_I)$ is **always** periodic in μ_I/T with period $2\pi/N_c$ always, and that the only difference between the low T and the high T phase should be a

- smooth, analytic periodic behaviour at low T, as predicted from a strong coupling calculation
- non-analytic periodic behaviour at high T, as predicted from a weak coupling calculation, with phase transitions at $\frac{\mu_I}{T} = \frac{2\pi}{N_c}(k + 1/2)$

This is an interesting prediction to be verified by lattice simulations.

2 – Numerical Results

2.1 – Simulation parameters

We have studied QCD with four degenerate staggered flavours of bare mass $a \cdot m = 0.05$ on a $16^4 \times 4$ lattice. The temperature is given by $T = 1/(N_t a)$, with $N_t = 4$ in our case. So $\theta = \mu_I/T = 4a\mu_I$.

With 4 flavours the exact Hybrid Monte Carlo algorithm can be used, with slight modifications needed to introduce the imaginary chemical potential.

At $\mu = 0$, a first order phase transition is present at $\beta_c \simeq 5.04$ (F.R. Brown *et al*, 1990).

Simulations have been performed on the QUADRICS machines of the ENEA Computer Center.

2.2 – The Polyakov loop with an imaginary μ

In pure gauge theory the expectation value of the Polyakov loop, $P(\vec{x}) \equiv |P(\vec{x})|e^{i\phi}$, is different from zero only in the deconfined phase, where the center symmetry Z_3 is spontaneously broken and $\langle\phi\rangle = 2k\pi/3$.

With dynamical fermions, $P(\vec{x})$ enters explicitely the fermionic determinant, $\det M[U]$, and Z_3 is broken: the effect of the determinant is like that of an external magnetic field which aligns $P(\vec{x})$ along $\langle\phi\rangle = 0$. At high T the Z_3 degeneracy is removed and $\langle\phi\rangle = 0$ is the true vacuum.

At $\mu_I \neq 0$, what enters $\det M[U]$ is not $P(\vec{x})$, but $P(\vec{x})e^{i\theta}$, $\theta \equiv \frac{\mu_I}{T}$. The determinant now tends to align $\langle\phi\rangle + \theta$ along zero, like a magnetic field pointing in the $-\theta$ direction, and one expects $\langle\phi\rangle = -\theta$ at low T

At high T the fermionic determinant still lifts the Z_3 degeneracy, but it is θ that fixes which is vacuum. For $(k - \frac{1}{2}) < \frac{3}{2\pi}\theta < (k + \frac{1}{2})$ one expects $\langle\phi\rangle \sim \frac{2k\pi}{3}$ and $\theta = 2(k + \frac{1}{2})\pi/3$ should correspond to phase transitions from one Z_3 sector to the other (i.e. the RW phase transitions).

In the following figure we report the average value of the Polyakov loop phase as a function of the imaginary chemical potential for different values of β.

2.3 – Polyakov loop phase

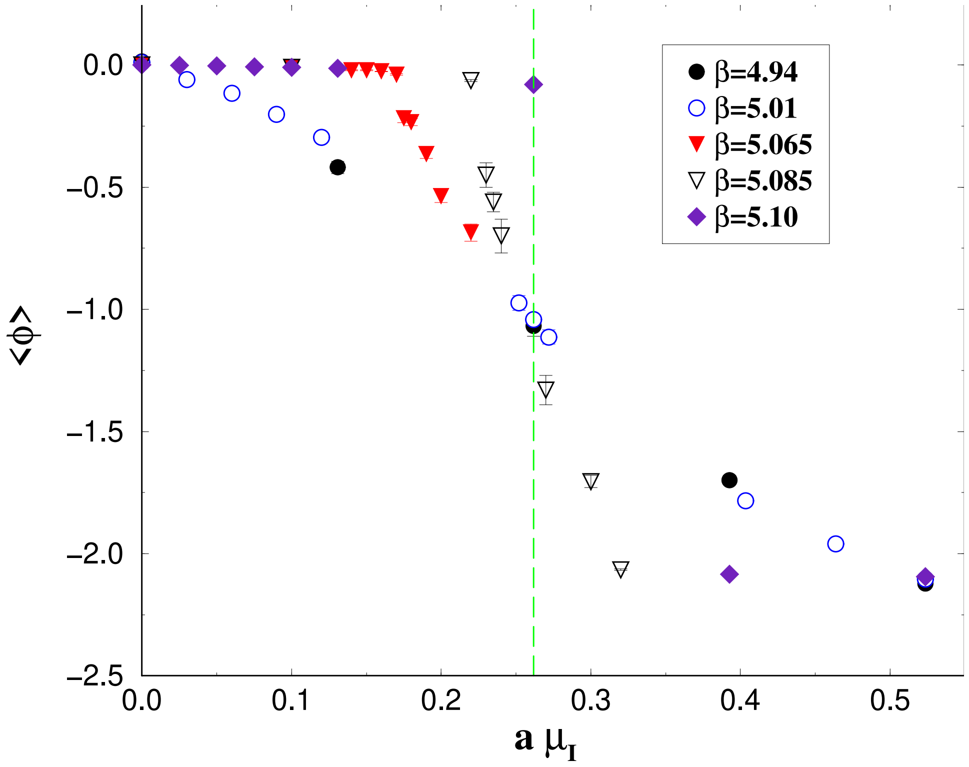

The vertical dashed line corresponds to $\theta = \mu_I/T = \pi/3$.

- For $\beta = 4.94, 5.01 < \beta_c$, $\langle\phi\rangle$ is continuous in μ_I and $\langle\phi\rangle \simeq -\theta$
- For $\beta = 5.10 > \beta_c$, $\langle\phi\rangle \simeq 0$ as long as $\theta < \frac{\pi}{3}$. For $\theta > \frac{\pi}{3}$ there is a sudden change to $\langle\phi\rangle \simeq -\frac{\pi}{3}$: we are crossing the Roberge-Weiss (RW) phase transition from one Z_3 sector to the other.
- At intermediate values, $\beta = 5.065$ and 5.085, $\langle\phi\rangle \simeq 0$ until a critical value of μ_I, where it starts moving almost linearly crossing continuously the Z_3 boundary: this does not correspond to the RW phase transition but rather to the crossing of the chiral critical line, i.e. the continuation in the T–μ_I plane of the chiral phase transition.

2.4 – Chiral condensate

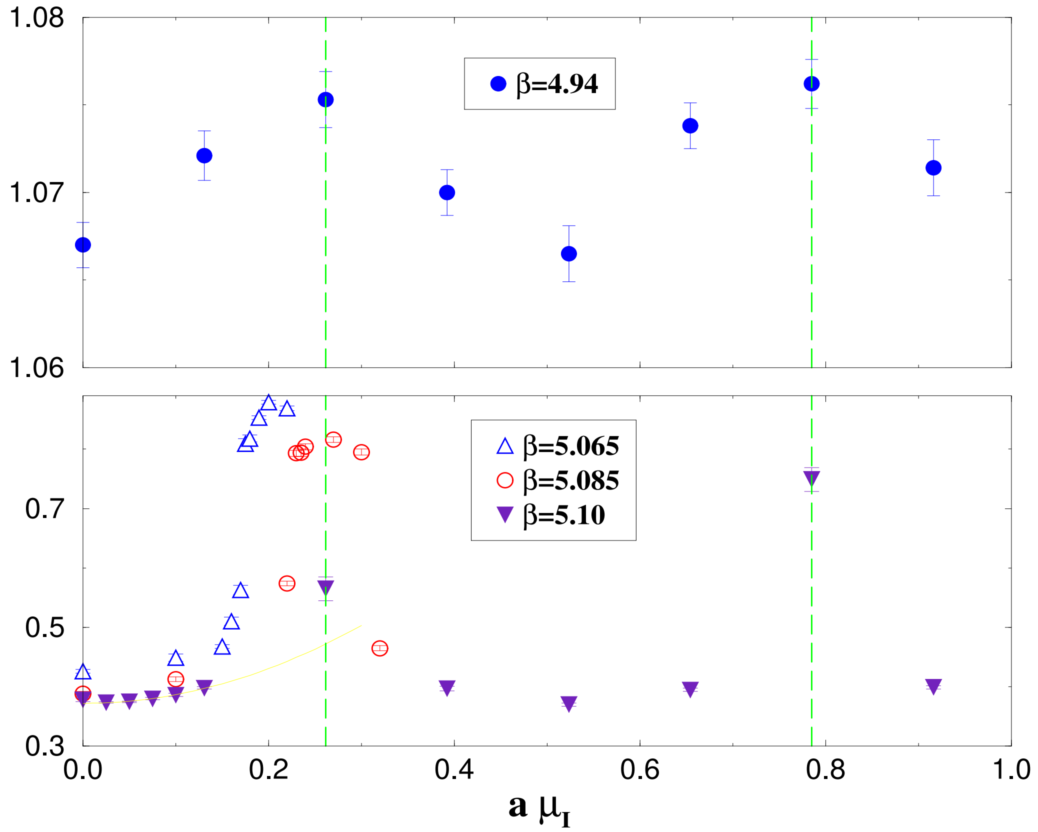

We display in the figure our results for the chiral condensate. The green vertical dashed lines correspond to $\theta = \frac{\pi}{3}$ and $\theta = \pi$.

Symmetries of $\langle\bar{\psi}\psi\rangle$: it must be periodic $\frac{2\pi}{3}$ in $\theta = N_t a \mu_I$ and, like the partition function, an even function of μ_I $\longrightarrow$ we expect symmetry around all points $\theta = n\pi/3$. This is verified in our data.

For $\beta < \beta_c$, $\langle\bar{\psi}\psi\rangle$ is continuous in μ_I. At $\beta = 5.065$ there is a critical value $a\mu_I \simeq 0.17$ above which the theory has a transition to a spontaneously broken chiral symmetry phase: we are crossing the chiral critical line. At $\beta = 5.085$ this happens at $a\mu_I \simeq 0.22$ and as we increase μ_I, we observe a transition back to the chirally restored phase at $a\mu_I \simeq 0.30$, which is the symmetric point with respect to $\theta = \frac{\pi}{3}$.

At $\beta = 5.10$ we do not cross, when changing μ_I, the chiral critical line, but the RW critical lines.

2.5 – Imaginary part of the baryon density

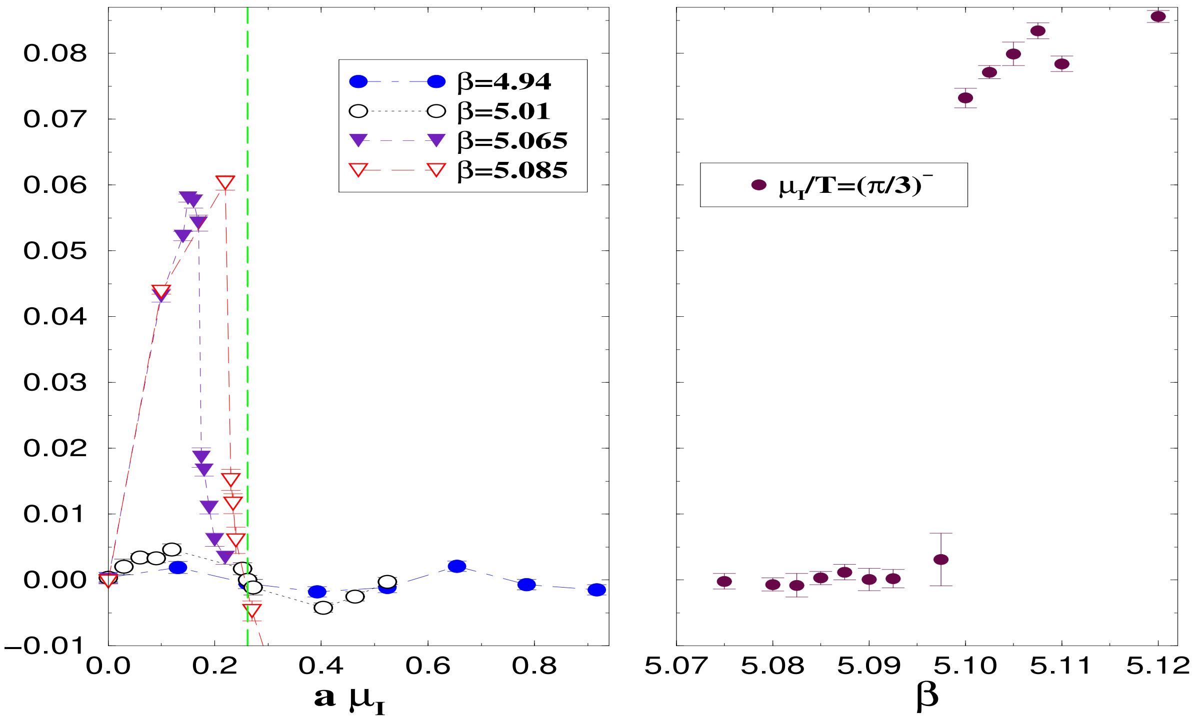

Symmetries of the baryon density $\langle b\rangle$: It is an odd function of μ, therefore, for $\mu = i\mu_I$, $\langle b\rangle$ is also purely imaginary and odd. This, combined with the periodicity in μ_I, leads to $\langle b\rangle(\theta = \frac{\pi}{3}^-) = -\langle b\rangle(\theta = \frac{\pi}{3}^+)$. This implies $\langle b\rangle = 0$ at $\theta = \pi/3$, unless $\langle b\rangle$ is not continuous on that point. Thus $\langle b\rangle \neq 0$ at $\theta = \frac{\pi}{3}^\pm$ implies the presence of the RW critical line.

On the right hand side of the figure Im $\langle b\rangle$ at $\theta = \frac{\pi}{3}^-$ is plotted as a function of β: the transition to $\langle b\rangle \neq 0$ fixes the endpoint $\beta_E = 5.097(2)$ of the RW critical line. At β_E the chiral condensate has a transition as well: this implies that the RW critical line ends on the chiral critical line.

On the left hand side we show Im$\langle b\rangle$ as a function of μ_I for different values of $\beta < \beta_E$, the green vertical dashed line corresponds to $\theta = \frac{\pi}{3}$: $\langle b\rangle$ is always zero and continuous at $\theta = \frac{\pi}{3}$, but it is interesting to note how it starts developing the discontinuity as $\beta \to \beta_E$.

2.6 – Phase diagram

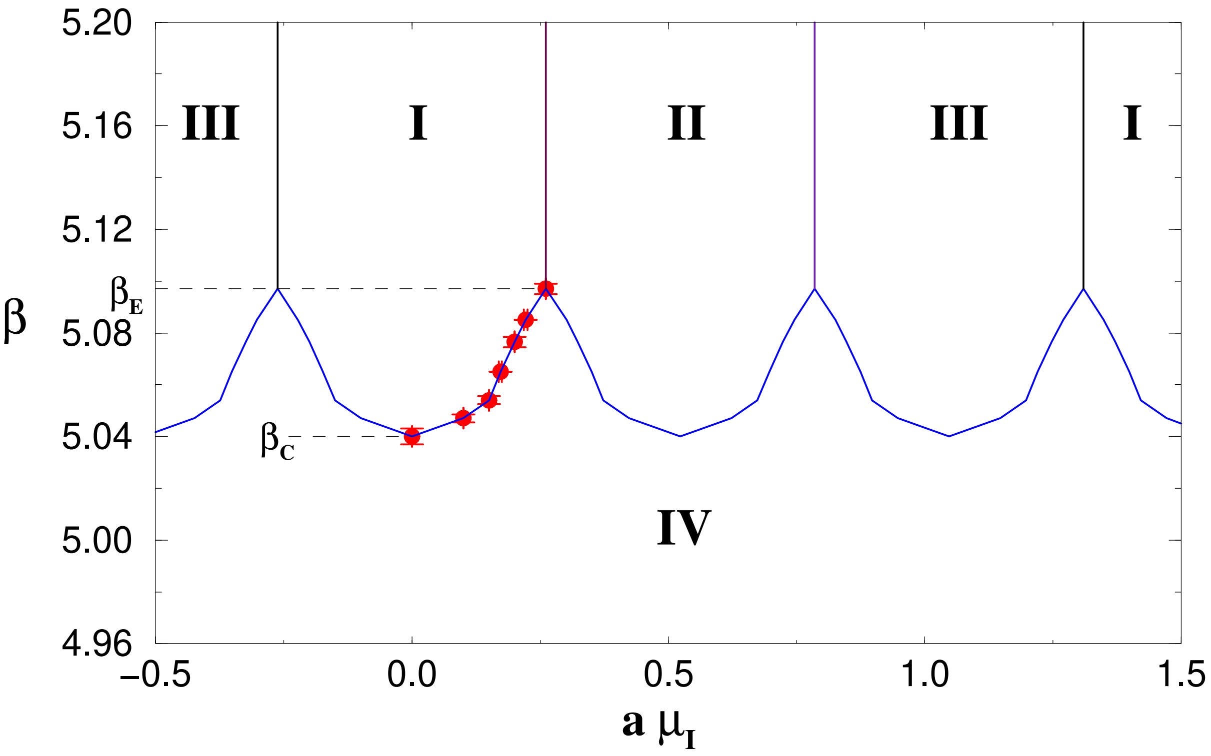

This is a sketch of the phase diagram in the β–μ_I plane, as emerges from our data. Since the temperature $T = \frac{1}{N_t a(\beta)}$ is a monotonic increasing function of β, this is analogous to the T–μ_I phase diagram.

The red points correspond to our determinations of the chiral critical line, obtained either changing β at fixed μ_I or changing μ_I at fixed β. The rest of the chiral critical line has been obtained by interpolating our determinations and by extending to the whole range of μ_I by exploiting the symmetries of the partition function.

The chiral critical line separates region IV from other regions, while the RW critical lines separate regions I,II and III among themselves. We have verified that the RW critical lines end right on the chiral critical lines, and that the chiral critical line continues to be first order, as it is at zero density, also at $\mu_I \neq 0$.

At $\mu_I = 0$, $\beta_c = 5.040(20)$, in agreement with (F.R. Brown *et al*, 1990). We can translate our determinations of $\beta_c(\mu_I)$ into determinations of $T_c(\mu_I)/T_c(0)$ by using the relation

$$\frac{T_c(\mu_I)}{T_c(0)} = \frac{a(\beta_c(0))}{a(\beta_c(\mu_I))} \tag{7}$$

The ratio of lattice spacings at different β's can be obtained using the 2–loop beta function.

2.7 – Analytic continuation of the critical line

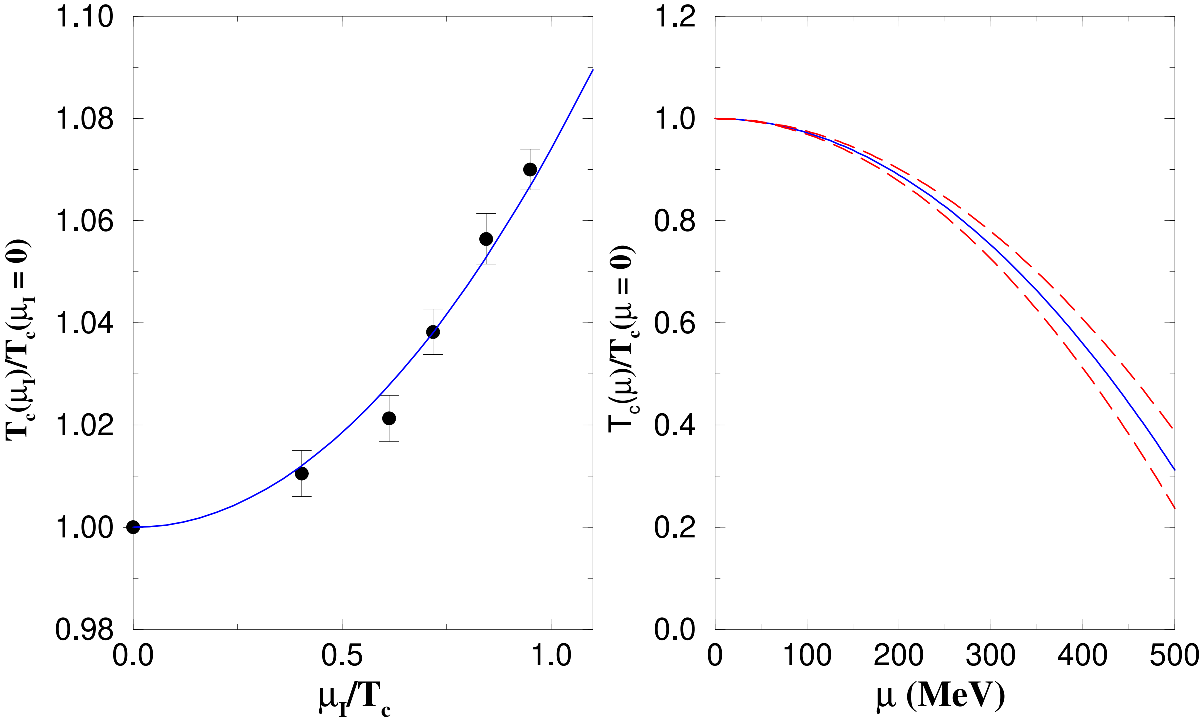

On the left we show our determinations of $T_c(\mu_I)/T_c(0)$ for the chiral critical line. With the aim of performing the analytic continuation to real chemical potential, we have tried a quadratic fit to our data. Our best fit, corresponding in the figure to the continuos line, is

$$\frac{T_c(\mu_I)}{T_c(0)} = 1 + 0.074(5)\left(\frac{\mu_I}{T_c}\right)^2 \tag{8}$$

with a χ^2/d.o.f. = 0.9. Our data are not precise enough to permit a determination of the quartic and higher order terms.

The analytic continuation of our fitted chiral critical line into the T – real chemical potential plane is shown on the right hand side. The continuous line corresponds to the central value of the fit, while the dashed lines give an indication of the error.

3 – Conclusions

We have studied finite temperature QCD with 4 flavours of dynamical staggered flavours with a degenerate mass $am = 0.05$ and an imaginary chemical potential. Our results can be summarized as follows:

- We have determined the phase structure in the T–imaginary chemical potential plane. In particular we have confirmed the existence of the RW critical lines, located their endpoints and assessed their interplay with the chiral critical line. We have also assessed the first order nature of the chiral critical line.
- We have studied the analytic continuation to real chemical potential. In particular we have studied the continuation of the chiral critical line and compared our results with those obtained by the same method in the two flavour case (de Forcrand and Philipsen) and by reweighting techniques in the four flavour case (Fodor and Katz).

We plan to extend in the future our study to the relevant physical case of $2 + 1$ flavours.

As a final comment, we notice that the physical interesting region of high temperature and small chemical potential can now be studied by essentially three techniques:

1) Direct calculations of derivatives
2) Reweighting
3) Analytic continuation from imaginary μ

Cross checks among the three different approaches should produce reliable physical results in the near future.